PNAS RESEARCH ARTICLE | BIOPHYSICS AND COMPUTATIONAL BIOLOGY

Quasiuniversal scaling in mouse-brain neuronal activity stems from edge-of-instability critical dynamics

Guillermo B. Morales[a], Serena di Santo[b], and Miguel A. Muñoz[a,1]

Edited by Terrence Sejnowski, Salk Institute for Biological Studies, La Jolla, CA; received June 6, 2022; accepted December 31, 2022

The brain is in a state of perpetual reverberant neural activity, even in the absence of specific tasks or stimuli. Shedding light on the origin and functional significance of such a dynamical state is essential to understanding how the brain transmits, processes, and stores information. An inspiring, albeit controversial, conjecture proposes that some statistical characteristics of empirically observed neuronal activity can be understood by assuming that brain networks operate in a dynamical regime with features, including the emergence of scale invariance, resembling those seen typically near phase transitions. Here, we present a data-driven analysis based on simultaneous high-throughput recordings of the activity of thousands of individual neurons in various regions of the mouse brain. To analyze these data, we construct a unified theoretical framework that synergistically combines a phenomenological renormalization group approach and techniques that infer the general dynamical state of a neural population, while designing complementary tools. This strategy allows us to uncover strong signatures of scale invariance that are "quasiuniversal" across brain regions and experiments, revealing that all the analyzed areas operate, to a greater or lesser extent, near the edge of instability.

criticality | neuroscience | scaling | renormalization group

Significance

Advancing our knowledge of how the brain processes information remains a key challenge in neuroscience. Importantly, the brain, even at rest, is in an energetically costly state of ongoing activity, whose origin and meaning still need to be fully elucidated. An inspiring hypothesis suggests that such activity is generated by an underlying critical dynamics, at the edge between order and disorder. Here, we combine existing approaches that have not been investigated side by side before, including a phenomenological renormalization group approach and disordered-systems techniques, to quantitatively analyze experimental datasets of thousands of simultaneously recorded neurons across the mouse brain. We find strong signatures of scaling and near-to-critical behavior across regions, shedding new light onto the meaning of ongoing brain activity.

The brain of mammals is in a state of continuous ongoing activity even in the absence of stimuli or specific tasks (1–3). Shedding light on the origin and functional meaning of such an energy-demanding baseline state of background dynamics and its interplay with input-evoked activity are challenging goals, essential to ultimately understand how different brain regions represent, process, and transmit information (4–6). Following the fast-paced development of powerful neuroimaging and electrophysiological technologies such as two-photon calcium imaging (7) and neuropixels probes (8), recent years have witnessed important advances in our understanding of these issues.

An inspiring hypothesis—which aims to become a general principle of brain dynamical organization—posits that neuronal networks could achieve crucial functional advantages, including optimal information processing and transmission, by operating in the vicinity of a critical point (9–15). Using the jargon of statistical physics, this implies that the network operates in an intermediate regime at the border between "ordered" and "disordered" phases (9, 12, 16–25). Criticality, with its concomitant power-laws has been hypothesized to entail functional advantages for information processing such as, e.g., an exquisite sensitivity to perturbations and a huge dynamic range (13, 16) to name a few. Moreover, it also gives rise to the emergence of a broad spectrum of spatio-temporal scales, i.e., scale invariance or simply "scaling" (13, 26, 27).

In spite of its conceptual appeal and thrilling implications, the validity of this so-called "criticality hypothesis" as an overarching principle of dynamical brain organization remains a controversial issue (see, e.g., refs. 28–30). Therefore, novel theoretical approaches and more-stringent experimental tests are much needed to either prove or disprove this conjecture and, more in general, to advance our understanding of the mechanisms underlying brain ongoing activity.

From the theoretical side, it is crucial to refine the conjecture itself and discern what type of criticality is the most pertinent to describe brain activity (10, 13). Different possible scenarios have been explored; among them (13): i) the edge of activity propagation, with scale-free avalanching behavior (9, 12, 18, 31), ii) the edge of a synchronization phase transition (13, 25, 32–35), iii) the edge of a stable-unstable transition, often called "edge of chaos" but to which we will refer as "edge of instability" hereon (14, 15, 36, 37), and iv) statistical criticality (10, 38).

From the empirical side, evidence of putative brain criticality often relies on the observation of scale-free bursts of activity, called "neuronal avalanches" (9, 21, 33, 39–41), long-range spatio-temporal correlations (42, 43), statistical

Author contributions: G.B.M., S.d.S., and M.A.M. designed research; G.B.M., S.d.S., and M.A.M. performed research; G.B.M., S.d.S., and M.A.M. contributed new reagents/analytic tools; G.B.M. analyzed data; and G.B.M., S.d.S., and M.A.M. wrote the paper.

The authors declare no competing interest.

This article is a PNAS Direct Submission.

[1]To whom correspondence may be addressed. Email: mamunoz@onsager.ugr.es.

This article contains supporting information online at http://www.pnas.org/lookup/suppl/doi:10.1073/pnas.2208998120/-/DCSupplemental.

Published February 24, 2023.

critical-like patterns of activity (10, 38) the analysis of whole-brain models fitted to match empirically observed correlations (44–47), etc. Recently, with the advent of modern techniques enabling simultaneous recordings of thousands of neurons, complementary experimental evidence revealing the existence of scaling in brain activity—which might or might not stem from underlying criticality (10, 13, 30, 48)—has emerged from unexpected angles. Among these, let us mention i) a novel renormalization-group approach which identified strong signatures of scale-invariant activity in recordings of more than a thousand neurons in the mouse hippocampus (49–51), ii) the direct inference—using linear response theory and methods from the physics of disordered systems—of "edge-of-instability" type of critical behavior in neural recordings from the macaque monkey motor cortex (37), and iii) the discovery of an unexpected power-law distribution, which revealed scale invariance in the spectrum of the covariance-matrix from tens of thousands of neurons in the mouse visual cortex (6).

What all these works have in common, is the fact the they use specifically designed, powerful mathematical tools to analyze vast amounts of high-throughput data.

Here, we bring these diverse approaches to a common ground and develop complementary tools leveraging them synergistically in order to analyze state-of-the-art neural recordings in diverse areas of the mouse brain (52). As shown in what follows, these analyses strongly enhance our understanding of scale-invariance and possible criticality in the brain. In particular, they allow us to elucidate the emergence of quasiuniversal scaling across regions in the mouse brain and to conclude that all such regions are, to a greater or lesser extent, posed close to the edge of instability.

Theoretical Framework and Open-Ended Questions

For the sake of self-containedness, let us briefly discuss the three innovative theoretical approaches cited above, along with some open questions that we pose (further technical details are deferred to the *Methods*).

(A) Renormalization Group Approach to Neuronal Activity. The renormalization group (RG) is retained as one of the most powerful ideas in theoretical physics, allowing us to rationalize collective behavior—at broadly diverse observational scales—from the properties of the underlying "microscopic" components, and to understand, for instance, the emergence of scale invariance (27). In a remarkable contribution, Meshulam et al. developed a phenomenological RG approach to analyze time series from large populations of simultaneously recorded individual spiking neurons and scrutinize their collective behavior (49, 50). The method, similar in spirit to Kadanoff's blocks for spin systems (27), allows one to construct effective descriptions of time-dependent neural activity at progressively larger "coarse-grained" scales. Notably, a number of nontrivial features—generally attributed to scale-invariant critical systems—emerge from the application of such RG analyses to recordings of more than 1,000 neurons in the hippocampus while the mouse is moving in a virtual-reality environment. These features include among others: i) a non-Gaussian (fixed-point) distribution of neural activity at large scales, ii) nontrivial scaling of the activity variance and autocorrelation time as a function of the coarse-graining scale, and iii) a power-law decay of the spectrum of the covariance matrix (49, 50).

A limitation of this type of phenomenological RG analysis is that, even if it is capable of uncovering scale invariance, it does not allow discerning what kind of putative phase transition could be at its origin. Moreover, doubts have been raised about the possible interpretation of the results as stemming from criticality (see refs. 53 and 54 and below).

In any case, leaving aside for the time being these caveats, one can wonder whether the observed scaling features are shared by other brain regions or if they are instead specific to the mouse hippocampus. Is there any kind of universality or at least "quasiuniversality" (in the sense of scaling exponents showing limited variability) in the neural dynamics across brain regions despite their considerable anatomical and functional differences? Is it possible to find empirical evidence that allows us to discern whether the observed scaling actually stems from critical behavior?

(B) Inferring the Dynamical Regime from Neural Recordings. Dahmen et al. devised a general approach—based on linear-response theory ideas and tools from the physics of disordered systems—that allows one to infer the overall dynamical state of an empirically observed neuronal population (see also refs. 14 and 15). In particular, this theoretical approach permits us to estimate the distance to the "edge of instability" from empirical measurements of the mean and dispersion of "spike-count covariances" (also called "long-time-window" covariances) across pairs of recorded neurons (37). Straightforward application of this approach to neural recordings from motor cortex of awake macaque monkeys at rest strongly supports the idea that such a region operates in a critical regime with nearly unstable dynamics (37). Thus, one can wonder whether other brain regions—for instance, the hippocampus in (A)—can also be empirically proven to be similarly close to the edge of instability.

Moreover, recently, Hu and Sompolinsky went a step further and derived an analytical expression (based also on linear-response theory for large random networks) for the full spectrum of eigenvalues of the spike-count covariance matrix as a function of its distance to the edge of instability. This provides us with an alternative method to estimate the distance to the edge of instability from empirical data. In particular, these analyses reveal that the distribution of eigenvalues of the covariance matrix develops a power-law tail as the network approaches the edge of instability (55). The resulting nontrivial eigenvalue distribution stems from the recurrent network dynamics near the edge of instability (55) and it clearly differs from the Marchenko–Pastur law for the correlations of independent random units (56).

Thus, an alternative way to infer the distance to the edge-of-instability is to find the parameter value in the theoretical model that best fits the empirically determined spectrum of spike-count covariance matrices as obtained from actual data.

(C) Scaling in Optimal Input Representations. Stringer et al. (6) studied experimentally and theoretically the spectrum of the covariance matrix in neuronal populations in mouse primary visual cortex (VISp) while the mouse was exposed to a very large set of sequentially presented natural images (recording more than 10^4 neurons in parallel; *Methods*). From the resulting data, they found that the spectrum of the covariance matrix obeyed "an unexpected power law" (6): the n-th rank-ordered eigenvalue scaled as $n^{-\mu}$ with $\mu \gtrsim 1$ (although the exact value of this exponent could be dependent on the noise model assumed for the estimation, see ref. 57).

This power-law decay of the rank-ordered eigenspectrum was somehow surprising; the authors were expecting a much faster decay, as would correspond to a lower-dimensional representa-

tion of the visual inputs. Notice that, here, by "representation" one means neural activity that stems from or is correlated with sensory or task-related inputs. On the other hand, the term "dimension" is employed in the sense of "principal component analysis" (PCA) (58), where the dimension is the number of principal components required to explain a given percentage of the total variance; often but not always (6) most of the variability in neural data can be recapitulated in just a few principal components or dimensions (59).

Remarkably, Stringer et al. were also able to show that the power-law decay of the rank-ordered eigenvalues is not an artifact directly inherited from the statistics of the inputs, but instead, it could stem from a trade-off between the neural representation of visual inputs being as high-dimensional as possible (i.e., including a large number of nonnegligible components in a PCA analysis) and mathematically preserving its smoothness (i.e., its continuity and differentiability). As a simple illustration of this last abstract property, let us mention that the smoothness of the representation prevents, for instance, that tiny variations in the inputs dramatically alter the neural population activity, which translates into a more robust encoding (6).

Let us finally recall that common knowledge in statistical physics tells us that a power-law decay of the covariance-matrix spectrum (i.e., of the "propagator") is one of the most remarkable generic trademarks of critical behavior, emphasizing the emergence of a scale-free hierarchical organization of spatio-temporal correlations (27). Indeed, this spectrum is one of the objects studied in the phenomenological RG approach (A), revealing a power-law decay (for the mouse hippocampus) with an exponent $\mu < 1$ (49), which violates Stringer et al.'s bound for continuous neural representations ($\mu \gtrsim 1$).

The results by Stringer et al. trigger a cascade of questions: Is the empirically observed scaling of the spectrum of the covariance matrix a mere consequence of the external input being represented in an optimal way? In other words, does the covariance spectrum obey scaling also in the absence of inputs, i.e., for resting state or ongoing activity? Is intrinsic criticality in the network dynamics required to "excite" such a broad spectrum of modes supporting optimal input representations? How come the exponent μ measured by Meshulam et al. in the hippocampus is smaller than 1 in seeming contradiction with Stringer et al.'s predictions?

Summing up: While A) allows us to detect and scrutinize the presence of scaling in empirical recordings in a systematic and quantitative way, B) provides us with practical tools to infer the actual dynamical regime of the underlying neural network, thus paving the way to ascribe empirically reported scaling to edge-of-instability criticality, and C) sets the scene for relating criticality to so far unexplored possible functional advantages for optimal input representation.

In what follows, we use these methods in a synergetic way while developing complementary tools to scrutinize scale invariance and criticality across regions and across experiments in the mouse brain, thus providing data-driven answers to most of the previously raised questions.

Results

Most of the forthcoming analyses rely on the empirical electrophysiological data presented by Steinmetz et al. in (52), where the activity, $x(t)$, of thousands of individuals neurons (in particular, the precise times of their spikes) is simultaneously recorded at a high (200 Hz) resolution in several mouse brain regions (as illustrated in Fig. 1). These recordings include periods in which the mouse is performing some specific task and some in which it is in a "resting-state". Therefore, we first separate both types of time series and analyze the corresponding "resting-state" and "task-related" activity independently, paying special attention to the former. In addition, we also consider data from recordings of mouse VISp from Stringer et al. (6) (*Methods*). In all cases, we restrict our analyses to areas (as reported in Fig. 1) with at least $N = 128$ simultaneously recorded neurons.

Quasiuniversal Scaling Across Brain Regions. We first employ the phenomenological RG approach to scrutinize whether nontrivial scaling behavior, such as the one reported in (49, 50) for the CA1 region of mouse hippocampus, is observed in other areas of the mouse brain. For the sake of clarity, let us summarize the gist of the RG approach (further details in *Methods* as well as in refs. 49 and 50), along with our main results.

Following the spirit of Kadanoff's block, one seeks to perform a coarse graining of N "microscopic variables"—i.e., single-neuron activities in this case—to construct effective descriptions at progressively larger scales. Nevertheless, given the absence of detailed information about physical connections (synapses) between neurons, a criterion of maximal pairwise correlation (rather than the standard one of maximal proximity) is used to block together pairs of neurons in a sequential way (49). Let us remark that, for this, it is crucial to determine pairwise correlations in a careful and consistent way; this requires the choice of a suitable discrete time bin for each data set, for which we have devised an improved protocol (*SI Appendix*, *Time-Scale Determination in the Extended Methods*). In this way, the activity time series of the two most correlated neurons are added together

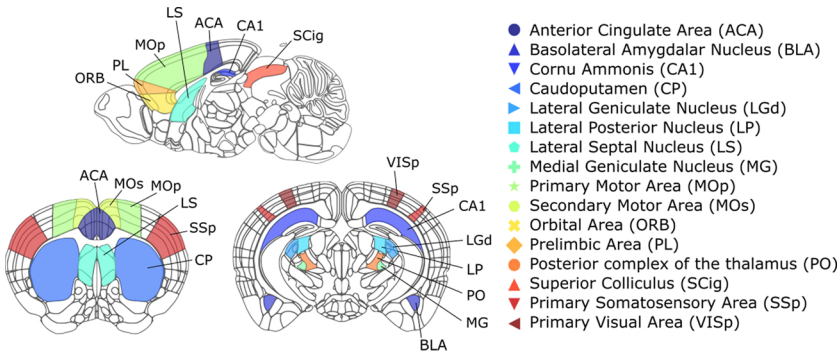

Fig. 1. Schematic representation of the regions in the mouse brain considered in this work (using three different projections), together with their names and corresponding acronyms. Credit: Allen Institute, Atlas brain maps: https://atlas.brain-map.org/atlas.

and properly normalized, giving rise to effective time series for "block-neurons" or simply "clusters" of size 2. One then proceeds with the second most-correlated pair of neurons and so on, until all neurons have been grouped in pairs. The process is then iterated in a recursive way, so that after k coarse-graining (RG) steps, there remain only $N_k = N/2^k$ block-neurons, each recapitulating the activity of $K = 2^k$ individual neurons.

The distributions of activity values across block-neurons at level k, $P_k(\{x\})$, can be then directly computed for the different steps of the RG clustering procedure, and from these distributions, a number of nontrivial features can be identified for all the considered mouse brain areas (52):

Non-Gaussian Probability Distribution of Block-Neuron Activity. Fig. 2*A* shows the probability distribution $Q_k(x)$ of nonzero activity values, x, of the coarse-grained block-neurons at one of the RG steps ($k = 5$, i.e., $K = 32$). Observe also, in the inset of Fig. 2*A*, the curve collapse obtained for sufficiently large values of K as well as the presence of significant non-Gaussian tails, as exemplified for one of the considered brain regions: the primary motor cortex (MOp). This convergence of $Q_k(x)$ to an asymptotic shape after a few RG steps, as observed for all regions (*SI Appendix*, Fig. S1), suggests that a nontrivial fixed point of the RG flow has been reached and that the emerging distribution of activity is rather universal across brain regions in resting conditions.

Scaling of the Activity Variance. As shown in Fig. 2*B* an almost perfect scaling is observed for the variance $M_2(K)$ of the nonnormalized activity of block neurons, with an average exponent $\overline{\alpha} = 1.38 \pm 0.08$ across regions. In particular, we measure $\alpha_{CA1} = 1.37 \pm 0.03 \pm 0.02$ (mean + mean-absolute-error of individual measurements + SD over experiments, *Methods*) for the CA1 region within the hippocampus, which is within errorbars of the value $\alpha = 1.56 \pm 0.07 \pm 0.16$ reported in ref. 50 for the same area. Notice that all these exponent values are always in between the expected ones for uncorrelated ($\alpha = 1$) and fully correlated variables ($\alpha = 2$), revealing consistently the existence of nontrivial scale-invariant correlations.

Scaling of the "Free Energy". This is defined as $F(K) = -\log(S_K)$, where S_K is the probability for a block-neuron of size K to be silent within a time bin. As shown in Fig. 2*C*, this quantity exhibits a clear scaling with cluster size, with an average exponent $\overline{\beta} = 0.79 \pm 0.03$ across regions ($0.78 \pm 0.04 \pm 0.05$ for CA1, to be compared with the value $0.87 \pm 0.014 \pm 0.015$ reported in ref. 50).

Scaling of the Autocorrelation Time. Fig. 2*D* shows that despite the very broad variability of intrinsic timescales for individual neurons within each region (*SI Appendix*, Fig. S4), dynamical scaling can be observed in the decay of the block-neuron autocorrelation times $\tau_c(K)$ (*Methods*) in all regions, with an average exponent across regions $\overline{z} = 0.22 \pm 0.05$ (with $z_{CA1} = 0.18 \pm 0.03 \pm 0.01$ for CA1, in perfect agreement with the one reported in ref. 50 for this region ($z = 0.22 \pm 0.08 \pm 0.10$) and compatible also with the exponent values reported in ref. 48 using a different approach). As an additional test for dynamical scaling, we show in (*SI Appendix*, Figs. S2 and S3) how the curves for the autocorrelation functions at different coarse-graining levels collapse when time is appropriately rescaled (as also illustrated in Fig. 2*D*, inset).

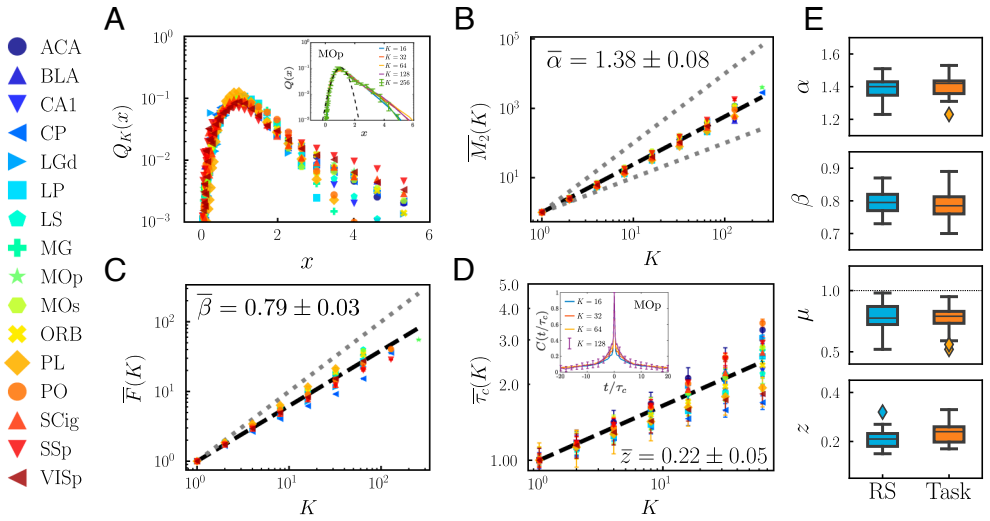

Fig. 2. Results of the phenomenological RG analyses of brain activity measured in 16 different mouse brain areas (*A–D* resting state activity). (*A*) Probability distribution for normalized nonzero activity in block-neurons of size $K = 32$ across brain regions (main panel), as well as (inset) at 5 consecutive steps of the coarse-graining for a representative region (MOp). (*B*) Variance of the nonnormalized activity as a function of the block-neuron size, K, in double logarithmic scale (upper and bottom dotted lines, with slopes 2 and 1, mark the fully correlated and independent limit cases, respectively). (*C*) Scaling of the free energy F_K as defined in *Methods* (the dotted line corresponds to the expected behavior for uncorrelated variables). (*D*) Inset: Decay of the autocorrelation function as a function of the rescaled time t/τ_C for the MOp region; a different value of τ_C is used for each cluster size but, after rescaling, all data collapse into a common curve. Main plot: scaling of the characteristic correlation time τ_C as a function of K in double logarithmic scale for the different areas. To facilitate the comparison between areas with different numbers of neurons, the variance has been normalized as $\overline{M_2}(K) = M_2(K)/M_2(K = 1)$, the probability of being silent rescaled to $\overline{F}(K) = F(K)/F(K = 1)$ and the correlation time as $\overline{\tau_C}(K) = \tau_C(K)/\tau_C(K = 2)$. In *B–D*, errorbars are computed as the standard deviation across split-quarters of data, with lengths typically smaller than the marker size. (*E*) Comparison of the exponent values α, β, μ, and z for resting-state (RS) and task-related activity (Task). Horizontal line inside each box represents the sample median across regions, the whiskers reach the nonoutlier maximum and minimum values, and the distance between the top (upper quartile) and bottom (lower quartile) edges of each box is the interquartile range (IQR). Outliers are represented with a diamond marker. For the exponent μ, the critical value $\mu^c = 1$ has been marked with a dotted line.

Scaling of the Covariance-Matrix Spectrum. By diagonalizing the covariance matrix computed at different levels of coarse-graining, it is possible to analyze how their corresponding spectra decay with the rank of the eigenvalues and how their cutoffs change with cluster size. As illustrated in Fig. 3, in all the analyzed brain areas, there is a clear power-law scaling of the eigenvalues with the rank, with an average exponent across regions $\overline{\mu} = 0.84 \pm 0.14$, as well as a common dependence with the fractional rank ($rank/K$), the latter manifested in the collapse of the curves at different levels of coarse graining, much as in ref. 49. Likewise, the value reported in ref. 49 for CA1 ($\mu = 0.76 \pm 0.05 \pm 0.06$) is in perfect agreement with our measured value for the same region, $\mu_{CA1} = 0.78 \pm 0.08 \pm 0.02$. Although we will address this point later on, let us for now stress that μ is smaller or, at most, approximately equal to one in all regions, seemingly suggesting discontinuity of the neural representations (6).

For the sake of consistency, we have also verified that the reported exponent values exhibit little variability upon changes in the time-discretization bin, with the exception of the exponent μ, for which we observe an increase on longer time-scales beyond the typical inter-spike-interval of the population activity (*SI Appendix*, Fig. S7).

Moreover, as it turns out, similar signatures of scale-invariance to those reported for resting-state activity emerge in RG analyses of neural recordings obtained while the mice are performing a task (*SI Appendix*, *Datasets in Extended Methods* and (52) for more details). This similarity is illustrated in Fig. 2*E*, which shows how the dispersion and mean value of the scaling exponents across regions are not significantly altered ($P > 0.1$ on a two-sample t test for each exponent) when one compares resting-state and task-related activity (*SI Appendix*, Fig. S7).

Finally, as a control test, we verified that the nontrivial scaling features revealed by the RG analyses are lost for all areas when the correlation structure of the data is broken either by i) reshuffling the times of individual spikes in the time series; ii) shifting each individual time series by a random time span while keeping the sequence of spikes; or iii) shuffling spikes across neurons (*SI Appendix*, Figs. S12–S14).

Dynamical State of Resting-State Activity Across Brain Regions and Experiments. Despite the elegance and appeal of the RG results—as originally presented by Meshulam et al.—their straightforward interpretation as stemming from underlying criticality has been questioned (53, 54). In particular, similar scaling behavior was found to emerge in a (noncritical) model of uncoupled neurons exposed to latent correlated inputs (53), even if some level of tuning was required (*Discussion*). Thus, it is not guaranteed a priori that the scaling behavior we just found across brain regions stems from underlying criticality and the RG approach does not allow us to provide an answer to this question. Therefore, we resort to alternative methods to estimate the dynamical regime of each brain region from empirical data as described above (37, 55). For this, one needs to compute spike-count covariance values across pairs of neurons, which measure the pairwise correlations in time-integrated activity (i.e., the total number of spikes) across samples (*Methods*).

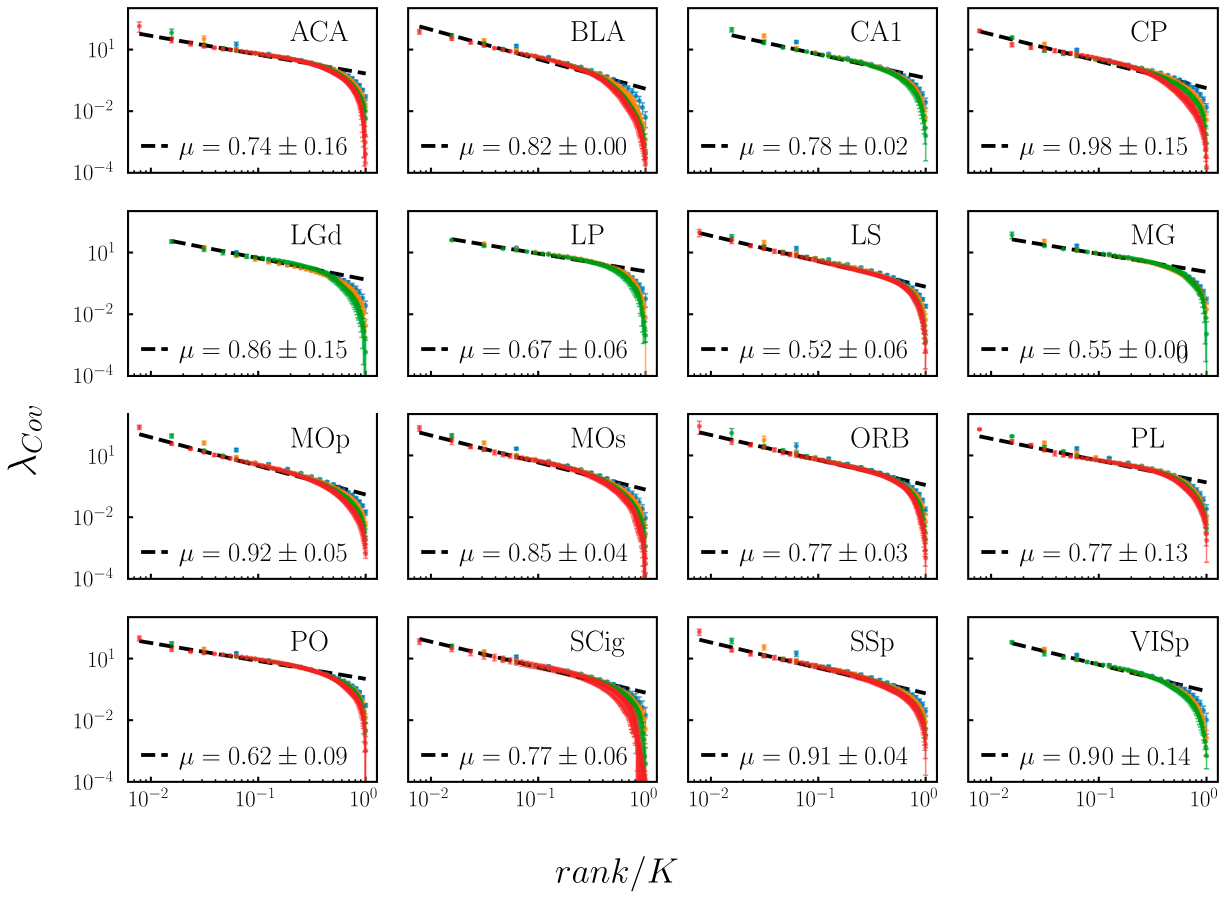

Fig. 3. Scaling of the covariance matrix spectrum for the resting-state activity in clusters of size $K = \{16, 32, 64, 128\}$ (blue, yellow, green, and red markers, respectively) in 16 different brain regions. Observe not only the decay of the rank-ordered eigenvalues as a power law of the rank but also the excellent collapse of the cutoffs obtained after rescaling the eigenvalue rank by the total size K. For each region, we collect the average powerlaw exponent and its SD across experiments, while errorbars (often smaller than the marker size) are computed as the SD across split-quarters of data (*SI Appendix*, Table S2).

In particular, to compute meaningful covariances, one assumes that neural activity is stationary, a condition that typically holds during recordings of resting-state type of activity, but not as much in task-related activity, for which network activity is inherently input-driven and nonstationary. Therefore, we restrict our forthcoming analyses to resting-state data (an augmented Dickey–Fuller test was performed to check for stationarity in all cases; *SI Appendix*, Table S1 and *Stationarity of Spiking Statistics in Extended Methods*).

We also notice that the values of spike-count covariances depend on the window sizes over which such counts are measured (37). In what follows, we take sampling windows of $T = 1s$, which are sufficient for autocorrelations to decay while maximizing the number of samples over which spike-count covariances are computed, thus limiting subsampling biases (Fig. 4*A* an *SI Appendix*, Table S1).

Using the so-obtained empirical values of pairwise spike-count covariances as measured for a given brain region, we now consider two alternative methods to infer the distance to the edge of instability of the underlying dynamical process. Both methods rely on reproducing the statistics of the empirically measured covariances by using a linear-response approximation.

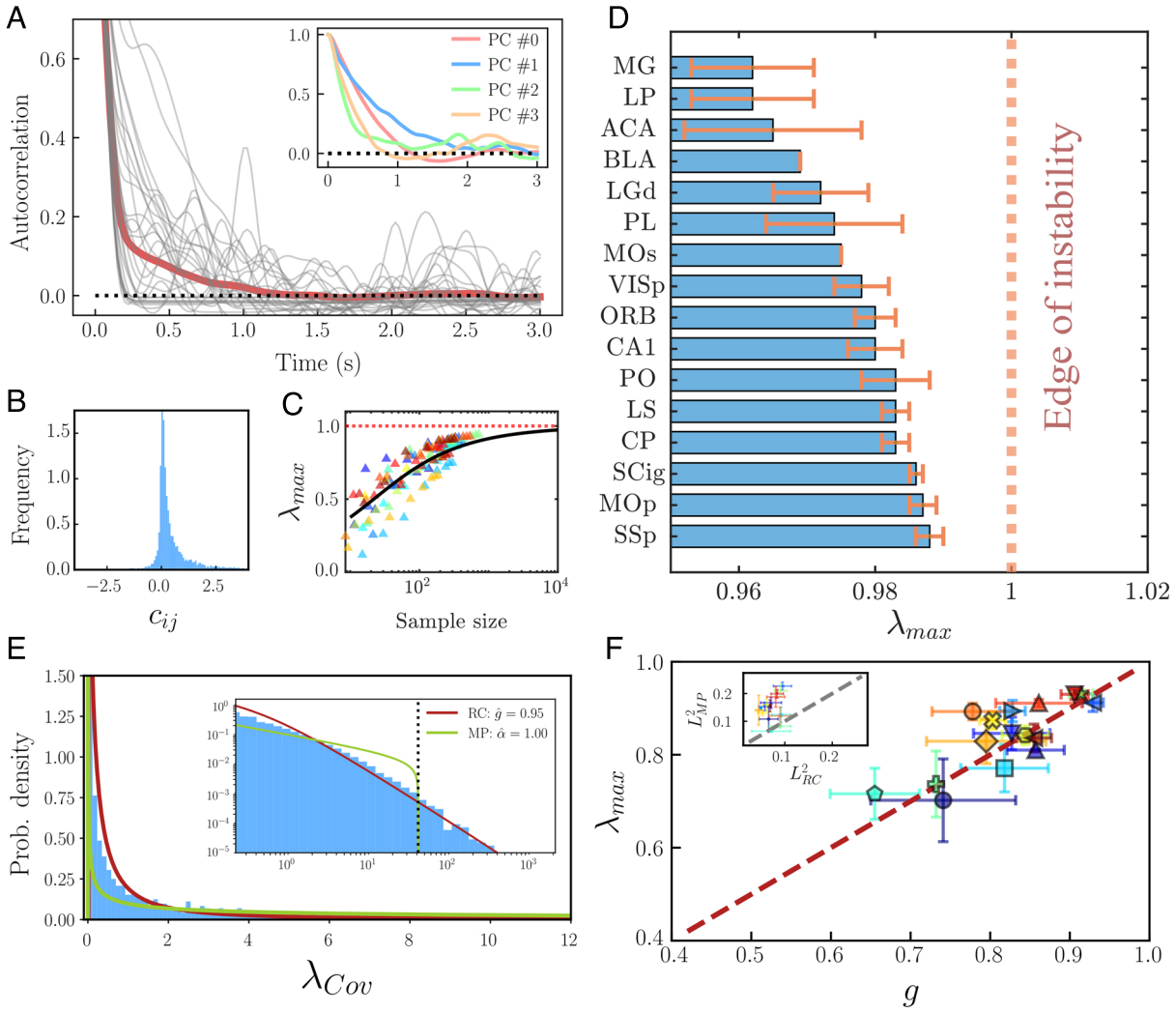

Fig. 4. (*A*) Autocorrelations decay in the MOp region (gray lines correspond to 30 randomly chosen neurons, while red line denotes the average across all neurons). Notice how autocorrelations vanish on a timescale of $\sim$ 1*s*. Inset: Decay of the average autocorrelation for the firing rates projected into the first four principal components. (*B*) Distribution of pairwise covariance values in one of the considered brain regions (MOp). Observe the strong peak around 0 (as expected from theoretical approaches of "balanced networks" (60)) as well as the large dispersion of values (37, 55), including (asymmetric) broad tails. (*C*) Dependence of the estimated value of λ_{max} on the number of neurons N in the sample. Each color corresponds to a region following the color code in Fig. 1; for each region, we show 10 points, corresponding to subsamples of 10% to 100% of the total neurons recorded, using the experiment with a greater number of recorded neurons for each area. Fitting the resulting values of λ_{max} for different values of N to Eq. **3** with a parameter Δ common to all regions and extrapolating for large values of N, one observes a fast convergence to the very edge of instability. (*D*) Proximity to criticality in 16 different regions of the mouse brain, as measured by the estimated largest eigenvalue λ_{max}—with $\lambda_{max} = 1$ marking the "edge of instability"—of the inferred connectivity matrix. The regions are ordered according to their average λ_{max} and the error bars are calculated as SD over different experiments in the same region. (*E*) Covariance eigenvalues distribution for an example region (MOp, blue histogram), together with the best-fitting Marchenko-Pastur (MP) distribution (green line, fitted parameter $\hat{\alpha} = 1.00$) and the best-fitting covariance eigenvalues distribution for a linear-rate model of randomly connected neurons (red line, fitted parameter $\hat{g} = 0.95$). Inset: Close-up of the empirical eigenvalue distribution and corresponding fits in a log–log scale. Notice how the theoretical expression derived in ref. 55 fits very well the long tail of large eigenvalues, whereas the MP distribution is upper bounded by $4\bar{\lambda}$, where $\bar{\lambda}$ is the mean value of the empirical distribution (black dotted line). (*F*) Estimated values of λ_{max} (first method, (37)) and g (second method (55)), including errorbars, for all the considered regions. Inset: Deviation of the empirical distribution to the Marchenko–Pastur (MP) distribution versus deviation to the theoretical distribution for a recurrent network (RC) of linear rate neurons close to the edge of instability.

In particular, one assumes a linearized response for each neuron i around a baseline state, i.e., a rate model:

$$\dot{x}_i(t) = -x_i(t) + g\sum_{i=1}^{N} J_{ij}x_j + \xi_i(t), \qquad [1]$$

where $\overline{\xi}(t)$ is a vector of zero-mean Gaussian white noises with $\langle \xi_i(t)\xi_j(t+\tau_0)\rangle = \delta_{ij}\delta(\tau_0)$ and J is the matrix of synaptic couplings, characterized by its mean (0) and variance $(1/N)$. The coupling parameter g sets the overall connection strength and, for this model, it also coincides with the spectral radius of the effective connectivity matrix $W \equiv gJ$; i.e., $\lambda_{max} = g$, where $\lambda_{max} = 1$ identifies the edge of instability. Importantly, the long-time window covariance (or zero-frequency covariance), $C_{ij} = \lim_{\Delta t\to\infty} \frac{1}{\Delta t}\langle \Delta s_i(t)\Delta s_j(t)\rangle$, with $\Delta s_i(t) = \int_t^{t+\Delta t}(x_i(t') - \langle x_i\rangle)dt'$, can be easily seen to be related to the connectivity matrix W via the simple matrix identity:

$$C = (I - W)^{-1}(I - W)^{-T}, \qquad [2]$$

where I is the identity matrix (55). This relation, which has been proven to be remarkably general, holds as a very good approximation for many different (nonlinear) models, including spiking neural networks ((37, 61, 62) and (63) for a recent review). Let us note that the entries of C can be estimated from empirical data as the covariances of the number of spikes in long-enough time windows (*Methods* and (37) for a more detailed explanation). Nevertheless, owing to strong subsampling problems, directly inverting the relation in Eq. **2** is not feasible and one needs to resort to the following advanced techniques to infer the value of g from empirically measured covariances.

(i) Estimations from the Statistics of Spike-Count-Covariance Distributions. As illustrated in Fig. 4*B* for one of the selected regions, the distribution of pairwise spike-count covariances is sharply peaked around 0, but it exhibits significant tails revealing the presence of heterogeneously correlated pairs. Recent work by Dahmen et al. (37)—relying on a dynamical mean-field approach and tools from the theory of disordered systems (such as spin glasses)—allows one to infer the spectral radius in Eq. **2** from empirically measured values of the mean $(\bar{c})$ and SD (δc) of such a distribution as

$$\lambda_{max} = \sqrt{1 - \sqrt{\frac{1}{1 + N\Delta^2}}}, \qquad [3]$$

where N is the total number of neurons in the population and $\Delta = (\delta c)/\bar{c}$ (see ref. 37 for details). In particular, this approach predicts that, for large spectral radii, the width of the covariance distribution is much larger than its mean in agreement with experimental observations.

As a warning, let us remark that the inferred value of λ_{max} strongly depends on the number of neurons being recorded and, since the available empirical data heavily subsamples each region, the aforementioned approach actually underestimates the real value of λ_{max}, which becomes much closer to 1 in the limit of tens of thousands of neurons (large N). Thus, in Fig. 4*C*, we plot the inferred values of λ_{max} as a function of the number of recorded cells, showing that the larger the neural population size, the larger the value of λ_{max}. Moreover, because of this dependence with the system size, it becomes difficult to compare the estimated values across regions with different numbers of neurons recorded. To avoid this limitation, we computed for each experiment and region the normalized covariance width, Δ, and then applied Eq. **3**, extrapolating to a common number of neurons $N = 10^4$. In Fig. 4*D*, we show the distance to the critical point thus estimated, with errorbars computed as the standard deviations across experiments in each region. Notice that most values lie on a very narrow window between 0.96 and 0.99, with a mean value $\overline{\lambda}_{max} = 0.978 \pm 0.009$, close to the edge of instability (*SI Appendix*, Table S1 and Fig. 4*F*).

(ii) Estimations from the Eigenvalue Spectrum of C. Hu and Sompolinsky (55) recently derived an analytical expression for the distribution of eigenvalues of the spike-count covariance matrix for a recurrent random network of linear rate neurons, whose dynamics follows Eq. **1**.

Their analytical expression—which is rather robust to subsampling effects—allows one to infer the network dynamical state by fitting the actual empirically determined spectrum to the theoretical distribution as a function of the only free parameter, g (*SI Appendix*, *Extended Methods* and ref. 55).

In particular, Fig. 4*E* shows the best fit ($g = 0.95$) of the empirically determined eigenvalue distribution for the MOp region to the Hu–Sompolinsky distribution, together with a (much worse) fit to the Marchenko–Pastur distribution (expected for random uncorrelated time series), thus emphasizing the nontrivial structure of the observed spike-count covariances, which stem from recurrent quasicritical interactions. A summary of the inferred g-values for all areas is shown in Fig. 4*F* (*SI Appendix*, Table S1), which further illustrates the strong similarity between the results obtained with the two employed methods, when the original number of neurons in each experiment is considered.

Nontrivial Scaling Features Emerge in the RG Analysis of Recurrent Random-Network Models at the Edge of Instability. To close the loop, we wondered whether a simple model of randomly coupled linear units, as the one defined by Eq. **1**, is able to reproduce other nontrivial scaling features as revealed by phenomenological-RG analyses, beyond the spectrum of covariances. In *SI Appendix*, Fig. S12, we show evidence that such recurrent neural networks driven by noise generate patterns of activity that reproduce many of the nontrivial scaling features emerging out of the RG analyses when they are posed close to the edge of instability (e.g., $g = 0.95$), while such nontrivial features are lost in the subcritical regime (where trivial Gaussian scaling emerges). In particular, the values of the exponents at the edge of instability ($\alpha \approx 1.28$, $z \approx 0.21$ and $\mu \approx 0.78$) are remarkably similar to the ones measured across regions in the mouse brain (*SI Appendix*, Table S2). The observation is rather striking given that these exponent values come from a linear model of randomly connected neurons, while real data are, most likely, generated by more complex nonlinear dynamics on heterogeneous networks. A recent work on universal aspects of brain dynamics (64) might help shedding light on this result.

Nonuniversal, Input-Dependent Exponents in Task-Related Activity. Saying that external stimuli shape neural correlations in information processing areas is, to a certain extent, an obvious statement. However, the fact that the spectrum of the activity covariance matrix follows a very simple mathematical rule that ultimately ensures the smoothness of the internal representation of inputs—as mathematically proved by Stringer et al. (6)—is quite remarkable. In particular, these authors showed that the neural representation for a d-dimensional (visual) input—that is to be encoded collectively in the neural activity of the primary visual cortex (VISp)—is constrained by the requirement of smoothness

of the representation (i.e., continuity and differentiability of the associated representation manifold) (6). Being more specific, for these conditions to hold, the spectrum of the covariance matrix needs to decay as a power-law with an exponent μ that must be greater than 1 for continuity, and greater than $1 + 2/d$—where d is the dimension of the input ensemble (*SI Appendix, Datasets in Extended Methods*)—for differentiability (6). Thus, for sufficiently "complex" inputs, i.e., with large dimensionality (d), this exponent is constrained to take a value arbitrarily close to (but larger than) unity, $\mu \gtrsim 1$.

On the other hand, in the previous RG analyses, we found values of μ consistently smaller than 1—both under resting conditions and in task-related activity—for all the considered areas (Fig. 3), in agreement with ref. 49, but in seeming contradiction with the predictions of Stringer et al. (6). How come that we report values $\mu < 1$ in all areas including sensory information encoding ones, even when the mouse is exposed to external stimuli? Does it mean that stimuli encoding violates the requirements for efficient representation put forward by Stringer et al. (6)?

At the core of this seeming paradox lies a data processing method proposed by Stringer et al. that allows one to extract the input-only related covariances from the overall "raw" covariance matrix (6). The approach stems from the idea that population activity can be decomposed into an input-related (or "input-encoding") subspace, which spans input-only related activity and a complementary space—orthogonal to the former one—which captures the remaining activity (65). In a nutshell, the so-called cross-validated PCA (cv-PCA) method consists in repeating twice the very same experiment and comparing the two resulting raw covariance matrices; this comparison allows one to infer which part of the covariance is shared by the two matrices and is, hence, input-related (*SI Appendix*, section 6) and which complementary part stems from unrelated background activity (6). Unfortunately, given the nature of such an experimental protocol, it is not possible to apply cv-PCA to the dataset of Steinmetz et al. (52), extensively employed above, to other areas.

However, to prove that our RG results above (consistent with $\mu < 1$) are not in contradiction with the ones by Stringer et al. ($\mu \geq 1$), we have extended the cv-PCA method (as explained in detail *SI Appendix*, section 6) to be able to actually extract from empirical data in ref. 6 not just the input-related covariance matrix but also the time-series of input-related neural activity. For this, the overall activity $x(t)$ of a given neuron at time t is projected into two separate subspaces, i.e., decomposed as

$$x(t) = \psi(t) + \epsilon(t), \qquad [4]$$

where $\psi(t)$ describes its input-related activity and $\epsilon(t)$ stands for the remaining "orthogonal" activity, responsible for trial-to-trial variability. This decomposition allows us to perform separate RG analyses to input-related and background activity data. As a consistency check, we also verified that the covariance-matrix eigenspectrum associated with $\psi(t)$ has no significant difference with the one obtained from the standard application of cv-PCA analyses in ref. 6 (*SI Appendix*, Fig. S16 for further details).

We now proceed to show the main results of applying the phenomenological RG approach over the data of ref. 6 considering i) the original timeseries $x(t)$, ii) the input-related activity $\psi(t)$, and iii) the background activity $\epsilon(t)$, with the results averaged over three different mice.

(i) Analyzing the original data (i.e., x variables), one observes again exponent values ($\alpha = 1.49 \pm 0.08$ and $\mu = 0.73 \pm 0.08$) in agreement with the previously reported quasiuniversal values for different mouse-brain areas (Fig. 5, together with *SI Appendix*, Fig. S8 and Table S1), highlighting the robustness of our results for very different recording techniques.

(ii) Considering the input-evoked activity (ψ) one finds that the exponent α—which was rather robust when measured from the overall activity data—is significantly altered (*SI Appendix*, Fig. S8). More importantly, a significant increase in the exponent μ is observed with respect to the original data analyses; it now respects the theoretical boundary $\mu > 1 + 2/d$ (with $d \longrightarrow \infty$ in natural images) for the smoothness of the representation manifold (Fig. 5). In addition, as also illustrated in Fig. 5, the value of μ obtained from our RG analyses decreases as the input dimensionality grows, in agreement with the theoretical results and empirical findings in ref. 6.

(iii) Finally, considering only the residual "orthogonal" parts (ϵ), we found slightly smaller values of μ with respect to the original-data analyses for the two types of inputs considered (Fig. 5). We notice, however, that this background activity is not to be confused with simple "white noise" as it exhibits correlations with a nontrivial power-law spectrum. When looking at the exponent α for the variance inside block-neurons, we did not observe a significant change with respect to the overall-activity case (*SI Appendix*, Fig. S8). This further supports the idea that the observed scaling exponents in the overall original-data are dominated by the higher-dimensional, background activity.

To summarize the previous results, Fig. 5 recaps the two observed trends in the scaling exponent μ. On the one hand—for data obtained using images of different intrinsic dimensionalities (*SI Appendix*, Extended Methods)—we found the relationship predicted and observed by Stringer et al. in ref. 6, namely that for the input-related activity ψ, the value of μ decreases with the complexity of the input signal, with a lower limit of $\mu = 1$ for high-dimensional inputs. On the other hand, the exponent μ decreases with the relative weight of background activity in the data: the more input-related activity that is projected away, the flatter the spectrum of the remaining orthogonal space.

As a side note, let us mention that—owing to the nature of the experimental setup in ref. 6, in which stimuli are interspersed with gray-screen interstimulus intervals—computation of actual dynamical correlations are not meaningful in this case, so that we purposely left aside the study of the dynamical scaling exponent z.

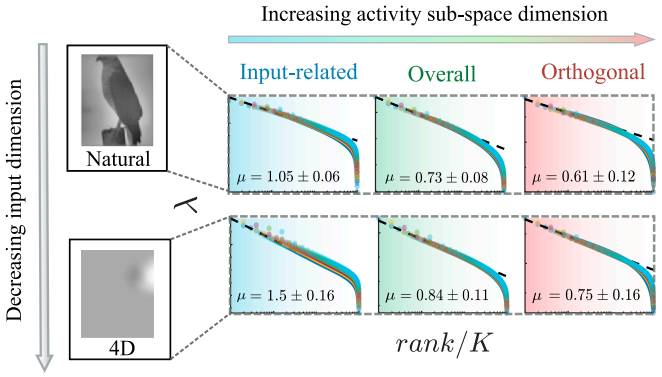

Fig. 5. Diagram showing the two observed trends in the power-law exponent μ, which characterizes the decay of the covariance-matrix eigenvalues as a function of their rank. μ decreases with the complexity of the input when activity is projected into the task-encoding subspace (also called representation manifold). On the other hand, for a fixed type of input, the exponent decreases with the proportion of background, "noisy" activity in the data, which lies in a higher-dimensional subspace orthogonal to the representational manifold. Natural and low-dimensional image examples have been adapted from ref. 6.

Likewise, the transformations carried on the overall data to extract the input-related and orthogonal activity do not necessarily preserve the biological significance of the zero-activity, making the computation of the "free-energy" exponent β pointless.

Thus, in summary, application of the phenomenological RG procedure to the data for VISp of Stringer et al. (6) reveals that the overall activity exhibits clear signatures of scale invariance, sharing its quasiuniversality with the previously analyzed regions, which relied on a different dataset. Nevertheless, this overall activity can be decomposed into input-related and noisy/orthogonal activities: the scaling exponent for the covariance matrix in the first case obeys the mathematical constraints derived by Stringer et al., thus solving the seeming contradiction with the spectrum of the overall data.

Discussion

Understanding how the brain copes with inputs from changing external environments, and how information from such inputs is transmitted, integrated, processed, and stored in a physical substrate consisting of noisy neurons—exposed also to a stream of other overlapping inputs—is one of the major challenges in neuroscience. The fast development of novel technologies that allow for the simultaneous recording of thousands of neurons paves the way to quantitative analyses of brain activity with unprecedented levels of resolution and detail, making it possible, for the first time, to discriminate between different overarching theories.

Here, we have taken advantage of high-throughput data, together with state-of-the-art theoretical approaches to analyze neuronal activity across regions and across experiments in the mouse brain. One of our chief objectives was to make progress in elucidating whether the so-called "criticality hypothesis"—in some of its possible formulations—is supported by empirical data. This goal has been tackled in two steps.

(i) The first step was to assess the presence or absence of scale invariance or "scaling" in neural data, for which we extensively rely on the phenomenological RG approach recently proposed by Meshulam et al. (49–51): Our analyses here confirm the existence of strong signatures of scaling in all the analyzed brain regions, with exponent values taking quasiuniversal values with only relatively small variations across experiments and areas (52). The level of universality is not as precise as in critical phenomena, i.e., in "nonliving matter" (though, even in Physics, critical exponents can take nonuniversal, continuously varying values depending, for instance, on structural heterogeneity/disorder (see, e.g., ref. 31).

A particularly relevant open question is thus whether the observed differences across regions can be related to the specific functional role of each area. Even if we do not have a clean-cut answer to this, let us make the following observation. One parsimonious measure of the role of a (mouse) brain area is its hierarchical score as recently determined (66), with low (high) scores corresponding to sensory (higher-level) areas. Results in Fig. 4*D* allow us to observe that sensory areas such as primary cortices MOp and SSp (with low scores; see e.g., Figure 6 in ref. 66) tend to operate closer to the edge of instability than secondary cortices (such as MOs) or areas in the prefrontal cortex (such as ORB, PL, and ACA). This seems to suggest that there could exist a relationship between the dynamical regime of a given area and its hierarchical score, with low-score regions being more "critical". On the other hand, we do not observe a clear and consistent trend in thalamic regions such as LGd, LP, MG, and PO. Thus, more thorough and comprehensive studies would be needed to draw solid conclusions on this possible connection between the dynamical regime and hierarchical score.

(ii) The second step was to scrutinize whether the empirically observed scale invariance stems from criticality or not. Thus, the next sections are devoted to the discussion of this hypothesis at the light of our results.

Criticality vs. Latent Dynamical Variables. Importantly, as already mentioned, recent works (53, 54) have shed doubts on the possible relation between the empirically found scaling in neural recordings and actual criticality, as originally suggested by Meshulam et al. (49, 50). In particular, Morrell et al. constructed a very simple model of binary neurons which, being uncoupled, cannot possibly exhibit collective behavior such as phase transitions or criticality (53). In their setup, all individual neurons are exposed to a large set of shared external, time-correlated inputs, so-called "latent dynamical variables" or simply "hidden variables". Surprisingly enough, such a toy model is able to reproduce—for a relatively broad region of the parameter space, but requiring some degree of fine tuning—the RG scaling with non-Gaussian activity distributions as well as a set of exponents roughly compatible with those in actual neural networks (with larger deviations for dynamical scaling) (49, 50). This suggests that the empirically observed scale invariance in neural recordings could possibly emerge as an evoked response to shared external drivings rather than stemming from critical dynamics (see however the discussion in ref. 38).

Let us recall that this type of dichotomy for the interpretation of scaling—between critical behavior on the one hand and a superposition of the simpler effects stemming from hidden variables on the other—is a common theme in different branches of science, being for example at the roots of discussions about the meaning of the Zipf's law in neural data (26, 30, 38, 67, 68).

Here, by employing a variety of tools, we have concluded that all the empirically analyzed brain regions lie—to a greater or lesser extent—at the edge of instability, i.e., in the vicinity of a critical point separating stable from linearly unstable phases. Moreover, we have also shown that a random network of linear units tuned close to the edge of instability suffices to reproduce nontrivial scaling features, with remarkably similar exponent values without the explicit need of external fields. Let us caution, however, that the previous results do not imply that external (latent) dynamical inputs may not have an impact on the recurrent dynamics nor on the observed scaling exponents. External inputs contribute to set the network working point at which covariances (as well as the stability matrix of the linear-rate model) are computed. Furthermore, the observed differences in exponent values across regions could stem from diverse exposures to latent fields from other areas. Further empirical and theoretical studies would be required to advance in this direction.

Edge of Instability and Optimal Representations. By applying the phenomenological RG procedure to the data for VISp from Stringer et al. (6), we found that the overall activity exhibits clear signatures of scale invariance and shares its quasiuniversality with the previously analyzed regions relying on a different dataset, solving a seeming contradiction between our own results for quasiuniversal scaling across brain regions and those in ref. 6. However, the projection of the overall or "raw" activity into input-representing and complementary/orthogonal space activities allowed us to conclude that the scaling exponent determined from RG analyses in the first case obeys the mathematical constraints derived by Stringer et al. Understanding how the

brain performs this task, i.e., how it separates signal from noise, is an open fundamental problem (see, e.g., ref. 69).

Let us also emphasize that given that all the analyzed regions are near critical, they are bound to exhibit power-law decaying covariance-matrix spectra. Thus, we conjecture that critical behavior creates a broad range of covariance scales, needed for neural networks to support optimal input representations with power-law decaying eigenvalues. More research is needed to confirm this conjecture and put it on firmer ground.

To further illustrate the possible relationship between power-laws in the spectra of covariance matrices and optimal input representations, let us mention that, in a related work, we have recently designed and analyzed a simple machine-learning model based on the paradigm of reservoir computing (70) to analyze this problem in a well-controlled example. This model consists of a recurrent network of coupled units/neurons, which receive shared external inputs, giving rise to reverberating activity within the network or "reservoir". Contrary to other machine-learning paradigms, the internal synaptic weights remain fixed during the training process: Only a smaller subset of links connecting to a set of readout nodes change during training, which makes reservoir-computing a versatile tool for diverse computational tasks (71). Inspired by the experiments of Stringer et al., we trained the network on an image classification task. We refer the interested reader to ref. 70 for further details. For our purposes here, it suffices to recall that the best performance is obtained when the tunable control parameters are set in such a way that the overall dynamical state is very close to, but below, the edge of instability. Moreover, within such an operational regime, the spectrum of the covariance matrix obeys the mathematical requirement for optimal representations, i.e., $\mu \gtrsim 1$, as observed for actual neural networks (6).

We find it quite suggestive that such a relatively simple artificial neural network becomes optimal in a regime that shares crucial statistical properties of the covariances with actual neural networks in the (mouse) brain. Thus, we believe that this machine-learning model may constitute a well-controlled starting point to further investigate the interplay between internal dynamics and external shared inputs in more realistic models of brain activity and to scrutinize optimal input representations.

Avalanche Criticality vs. Edge-of-Instability. As already discussed, we have found strong empirical evidence of critical behavior in the sense of vicinity to the edge of instability across brain regions. This type of behavior—called traditionally "edge of chaos" or "type-II criticality" in ref. 37—has long been (since the pioneering works of Langton and others (72, 73)) theoretically conjectured to be crucial for information processing in natural and artificial neural networks. In this case, edge-of-instability systems are characterized by the presence of many modes that are close to become unstable, and thus there is a large repertoire of possible dynamical states that can be excited, opening many possible channels to information processing and transmission in real time (13, 73, 74).

However, in the analyzed neural recordings, there are no large fluctuations in the overall level of global activity across time, in agreement with what was observed for the motor cortex of awake macaque monkeys in ref. 37 and with the expectation for "asynchronous states" in balanced networks (60). Nevertheless, it is noteworthy that in some other empirical observations, diverse levels of temporal variability in collective firing rates (i.e., oscillations) have been also reported together with the possibility of bursts and avalanching behavior (9, 39, 41). Actually, as stated in the Introduction, much attention has been previously paid to "avalanche criticality" (referred as "type-I criticality" in ref. 37), which is associated with networks in which there is an overall-activity mode about to become unstable, thus generating scale-free bursts of activity and possibly oscillations while the rest of modes remain stable (25, 33, 35). It should be emphasized that both types of criticality are not mutually exclusive as, in principle, it is possible to have a whole set of eigenvalues, including the overall-activity one, at the edge of instability. Thus, it seems a priori possible to construct computational models exhibiting both types of criticality in which the system can shift between different regimes depending on its needs. In our view, it is likely that actual brain networks exploit different ways of being critical to achieve diverse functional advantages for different tasks.

Conclusions

We have developed a synergistic framework which relies on recently proposed breakthrough approaches, but that also extends and combines them to analyze state-of-the-art recordings of the activity of many neurons across brain regions in the mouse. We find that all regions exhibit scale invariance and that all of them operate, to a greater or lesser extent, in a critical regime at the edge of instability. Moreover, we have argued that the resulting scaling in the spectrum of covariances might have important functional applications for information storage, as it facilitates the generation of optimal input representations. It is our hope that the present work stimulates further research on the remaining open questions and helps advance toward a more comprehensive understanding of the overall dynamics of brain networks and their emerging computational properties, as well as to disentangle universal and nonuniversal aspects across regions and behavioral states.

Materials and Methods

Phenomenological Renormalization-Group (RG) Approach. Let us briefly outline the phenomenological RG approach introduced in refs. 49 and 50. Given a set of N neurons, the empirically determined activity of the i-th neuron at a given time t_j is denoted by $\sigma_i(t_j)$, where $j \in (1, T)$ labels a discrete number of nonoverlapping time bins. Determining the most meaningful size of such time bins is an important technical aspect (Next section); here, we just assume that such an optimal time discretization is given.

As discussed in the main text, a criterion of maximal pairwise correlation is employed to group neurons together at each step k of the RG procedure. In particular, one considers the Pearson's correlation coefficients

$$C_{ij}^{(k)} = \langle \delta x_i^{(k)} \delta x_j^{(k)} \rangle / \sqrt{\langle (\delta x_i^{(k)})^2 \rangle \langle (\delta x_j^{(k)})^2 \rangle}, \quad [5]$$

where $\delta x_i^{(k)} = x_i^{(k)} - \langle x_i^{(k)} \rangle$ and $x_i^{(k)}$ is the activity of the block-neuron i at step k of the coarse-graining (we identify $x_i^{(0)} \equiv \sigma_i$ as the activity of neuron i before coarse-graining), while averages are computed across the available discrete time steps. At the beginning of each RG step, the two most correlated neurons, i and j_{*i}, are selected, and their activities are added into a new coarse-grained variable:

$$x_i^{(k+1)} = z_i^{(k)} \left(x_i^{(k)} + x_{j*i}^{(k)} \right), \quad [6]$$

where the normalization factor z_i^k is chosen in such a way that the average nonzero activity of the new variables x_i^{k+1} is equal to one. Notice that, owing to such a normalization criterion, activity values are not constrained to fulfill $x_i^k(t) < 1$. Then, one proceeds with the second most-correlated pair of neurons

and so on, until a set of N_k coarse-grained "block neurons", each containing the summed activity of $K = 2^k$ original neurons, has been constructed.

Iterating this procedure, after k steps there remain only $N_k = N/2^k$ coarse-grained variables or "block-neurons", $\{x_i^k\}_{i=1,2...N_k}$, each recapitulating the activity of $K = 2^k$ individual neurons. To figure out whether a fixed point of the RG flow exists, one can study the evolution of the probability density function for the activity of the coarse-grained variables, $P_K(x)$. Following (49), we separated $P_K(x)$ for block-neurons of size K in two components: the probability of being silent, S_K, and the probability $Q_K(x)$ of having nonzero activity x: $P_K(x) = S_K\delta(x) + (1 - S_K)Q_K(x)$. Trivially, if the original neurons were statistically independent, one would expect (as a direct consequence of the central limit theorem) to drive the activity distribution Q_K toward a Gaussian fixed-point of the RG flow. As pointed out in ref. 49, the RG convergence to a non-Gaussian fixed-point (i.e., invariance of the distribution across RG steps) reveals a nontrivial structure in the data.

Another quantity of interest is the variance of the activity distributions as a function of the size of the block neurons K:

$$M_2(K) = \frac{1}{N_k}\sum_{i=1}^{N_k}\left[\left\langle\left(\sigma_i^{(k)}\right)^2\right\rangle - \left\langle\left(\sigma_i^{(k)}\right)\right\rangle^2\right], \qquad [7]$$

where $\sigma_i^{(k)}$ is the summed activity of the original variables inside the cluster. Notice that, for totally independent variables, one would expect the variance to grow linearly in K (i.e., $M_2(K) \propto K$), whereas if variables were perfectly correlated $M_2(K) \propto K^2$. Nontrivial scaling is therefore characterized by $M_2(K) \propto K^\alpha$ with a certain intermediate value of the exponent $1 < \alpha < 2$.

On the other hand, $F_k = -\log(S_K)$ defines a sort of "free energy" for the coarse-grained variables at the k-th RG step (49). As more and more of the initial variables σ_i are grouped into cluster variables $x_i^{(k)}$, one would expect that the probability of having "silent" block-neurons (i.e., the probability that all neurons inside a cluster are silent) decreases exponentially with the size K of the clusters, leading to: $F(K) \propto K^\beta$ where $\beta = 1$ for initially independent variables.

One can also wonder whether there is some type of self-similarity in the dynamics at coarse-grained scales. Given that, commonly, fluctuations on larger spatial scales relax with a slower characteristic time scale, we should expect the time-lagged Pearson's correlation function (or simply autocorrelation function) of the coarse-grained variables to decay more slowly as we average over more neurons. In particular, for step k of the RG flow, one has

$$C^{(k)}(t) = \frac{1}{N_k}\sum_{i=1}^{N_k}\frac{\langle x_i^{(k)}(t_0)x_i^{(k)}(t_0+t)\rangle - \langle x_i^{(k)}\rangle^2}{\langle (x_i^{(k)})^2\rangle - \langle x_i^{(k)}\rangle^2}. \qquad [8]$$

Assuming that correlations decay exponentially in time with a characteristic time scale $\tau_c^{(k)}$ (i.e., $C^{(k)}(t) = e^{-t/\tau_c^{(k)}}$) at each coarse-graining level, dynamical scaling implies that the average correlation function collapses into a single curve when time is rescaled by the characteristic time scale: $C^{(k)}(t) = C(t/\tau_c^{(k)})$ and that this time scale obeys scaling with the cluster size: $\tau_c(K) \propto K^z$ where z is the dynamical scaling exponent. Finally, as argued in ref. 49, if correlations are self-similar, then we should see this by looking inside the clusters of size K. In particular, the eigenvalues of the covariance matrix, i.e., the propagator, which is scale-invariant at the fixed-point of the RG in systems with translational invariance (49) must obey a power-law dependence on the fractional rank: $\lambda = B\,(K/rank)^\mu$, where B is a constant and μ a decay exponent.

We estimate the goodness of each power-law fit by calculating the R-squared value, comparing with an equivalent exponential fit (*SI Appendix*, Fig. S10) (75). For the probability density of eigenvalues, we compute the log-likelihood ratios between the estimated power-law and alternative exponential and lognormal distributions (*Extended Methods* and *SI Appendix*, Tables S1 and S2).

Each exponent is expressed as $e = \bar{e} + MAE + \sigma$, where $\bar{e}$ is the average across different experiments (possibly from different mice), *MAE* is the mean-absolute-error, computed as the average across experiments of the experiment-specific errors measured over split-quarters of data, and σ is the SD across experiments (*SI Appendix*, Tables S1 and S2).

Measuring Covariances. Here, we use a general definition of covariance, as described by the following equation:

$$c_{ij}^S = \langle (x_i - \langle x_i\rangle)(x_j - \langle x_j\rangle)\rangle. \qquad [9]$$

During the RG analysis and in estimations of the distance to the edge of instability, the variable x_i represents the number of spikes in a time bin of width Δt, with averages taken over all timebins, so that c_{ij} measures the pairwise correlation of spike-count responses to repeated presentations of the same stimulus (or, in our case, repeated sampling of resting-state activity under identical behavioral conditions). Throughout this article, we referred simply as "covariance" when correlations were computed in the RG analysis using the time bin given by the geometric mean of neurons' ISIs, which renders time series where the average nonzero bin is populated by only one spike. In contrast, the term "long-time-window" or "spike-count" covariance is left for the distance to criticality analysis, in which $\Delta t = 1$s and the average nonzero bin in the time-series contains between 3 and 7 spikes, depending on the region. We notice that the later can also be written as the time integral of the time-lagged covariance $c_{ij}(\tau)$ (37):

$$c_{ij}^n = \lim_{\Delta t_0 \longrightarrow \infty}\int_{-\Delta t_0}^{\Delta t_0}\frac{\Delta t_0 - \tau}{\Delta t_0}c_{ij}^S(\tau)\,d\tau. \qquad [10]$$

which, loosely speaking, removes time-dependent effects and puts the emphasis onto pairwise heterogeneities.

Data, Materials, and Software Availability. Previously published data were used for this work (52).

ACKNOWLEDGMENTS. We acknowledge the Spanish Ministry and Agencia Estatal de investigación (AEI) through Project of I+D+i Ref. PID2020-113681GB-I00, financed by MICIN/AEI/10.13039/501100011033 and FEDER "A way to make Europe", as well as the Consejería de Conocimiento, Investigación Universidad, Junta de Andalucía and European Regional Development Fund, Project references A-FQM-175-UGR18 and P20-00173 for financial support. We also thank R. Calvo, C. Martorell, V. Buendía, P. Villegas, R. Corral, J. Pretel, P. Moretti, M. Ibañez, P. Garrido, and M. Marsili, for valuable discussions and/or suggestions on earlier versions of the manuscript.

Author affiliations: [a]Departamento de Electromagnetismo y Física de la Materia, Instituto Carlos I de Física Teórica y Computacional Universidad de Granada, Granada E-18071, Spain; and [b]Morton B. Zuckerman Mind Brain Behavior Institute Columbia University, New York, NY 10027

1. W. R. Softky, C. Koch, The highly irregular firing of cortical cells is inconsistent with temporal integration of random EPSPs. *J. Neurosci.* **13**, 334–350 (1993).
2. A. Arieli, A. Sterkin, A. Grinvald, A. Aertsen, Dynamics of ongoing activity: Explanation of the large variability in evoked cortical responses. *Science* **273**, 1868 (1996).
3. M. E. Raichle, The restless brain. *Brain Connect* **1**, 3–12 (2011).
4. G. Deco, V. K. Jirsa, P. A. Robinson, M. Breakspear, K. Friston, The dynamic brain: From spiking neurons to neural masses and cortical fields. *PLoS Comp. Biol.* **4**, e1000092 (2008).
5. C. Stringer *et al.*, Spontaneous behaviors drive multidimensional, brainwide activity. *Science* **364** (2019).
6. C. Stringer, M. Pachitariu, N. Steinmetz, M. Carandini, K. D. Harris, High-dimensional geometry of population responses in visual cortex. *Nature* **571**, 361–365 (2019).
7. C. Stosiek, O. Garaschuk, K. Holthoff, A. Konnerth, In vivo two-photon calcium imaging of neuronal networks. *Proc. Natl. Acad. Sci. U.S.A.* **100**, 7319–7324 (2003).
8. A. L. Juavinett, G. Bekheet, A. K. Churchland, Chronically implanted neuropixels probes enable high-yield recordings in freely moving mice. *Elife* **8**, e47188 (2019).
9. J. M. Beggs, D. Plenz, Neuronal avalanches in neocortical circuits. *J. Neurosci.* **23**, 11167–11177 (2003).
10. T. Mora, W. Bialek, Are biological systems poised at criticality? *J. Stat. Phys.* **144**, 268–302 (2011).

11. W. Bialek, *Biophysics: Searching for Principles* (Princeton University Press, 2012).
12. D. R. Chialvo, Emergent complex neural dynamics. *Nat. Phys.* **6**, 744–750 (2010).
13. M. A. Muñoz, Colloquium: Criticality and dynamical scaling in living systems. *Rev. Mod. Phys.* **90**, 031001 (2018).
14. L. M. Alonso *et al*., Dynamical criticality during induction of anesthesia in human ECoG recordings. *Front. Neural Circuits* **8**, 20 (2014).
15. G. Solovey *et al*., Loss of consciousness is associated with stabilization of cortical activity. *J. Neurosci.* **35**, 10866–10877 (2015).
16. W. L. Shew, D. Plenz, The functional benefits of criticality in the cortex. *Neuroscientist* **19**, 88–100 (2013).
17. S. Yu *et al*., Maintained avalanche dynamics during task-induced changes of neuronal activity in nonhuman primates. *Elife* **6**, e27119 (2017).
18. L. Cocchi, L. L. Gollo, A. Zalesky, M. Breakspear, Criticality in the brain: A synthesis of neurobiology, models and cognition. *Progr. Neurobiol.* (2017).
19. P. Massobrio, L. de Arcangelis, V. Pasquale, H. J. Jensen, D. Plenz, Criticality as a signature of healthy neural systems. *Front. Syst. Neurosci.* **9**, 22 (2015).
20. J. Wilting, V. Priesemann, 25 years of criticality in neuroscience-established results, open controversies, novel concepts. *Curr. Opin. Neurobiol.* **58**, 105–111 (2019).
21. D. Plenz *et al*., Self-organized criticality in the brain. *Front. Phys.* **9**, 639389 (2021), 10.3389/fphy.2021.639389.
22. A. Levina, J. M. Herrmann, T. Geisel, Dynamical synapses causing self-organized criticality in neural networks. *Nat. Phys.* **3**, 857–860 (2007).
23. M. Martinello *et al*., Neutral theory and scale-free neural dynamics. *Phys. Rev. X* **7**, 041071 (2017).
24. L. J. Fosque, R. V. Williams-García, J. M. Beggs, G. Ortiz, Evidence for quasicritical brain dynamics. *Phys. Rev. Lett.* **126**, 098101 (2021).
25. S. di Santo, P. Villegas, R. Burioni, M. A. Muñoz, Landau-Ginzburg theory of cortex dynamics: Scale-free avalanches emerge at the edge of synchronization. *Proc. Natl. Acad. Sci. U.S.A.* **115**, E1356–E1365 (2018).
26. M. E. Newman, Power laws, pareto distributions and Zipf's law. *Contemp. Phys.* **46**, 323–351 (2005).
27. J. J. Binney, N. J. Dowrick, A. J. Fisher, M. E. Newman, *The Theory of Critical Phenomena: An Introduction to the Renormalization Group* (Oxford University Press, 1992).
28. J. Touboul, A. Destexhe, Power-law statistics and universal scaling in the absence of criticality. *Phys. Rev. E* **95**, 012413 (2017).
29. J. M. Beggs, N. Timme, Being critical of criticality in the brain. *Front. Physiol.* **3**, 163 (2012).
30. R. J. Cubero, J. Jo, M. Marsili, Y. Roudi, J. Song, Statistical criticality arises in most informative representations. *J. Stat. Mech.: Theory Exp*. **2019**, 063402 (2019).
31. P. Moretti, M. A. Muñoz, Griffiths phases and the stretching of criticality in brain networks. *Nat. Commun.* **4**, 1–10 (2013).
32. H. Yang, W. L. Shew, R. Roy, D. Plenz, Maximal variability of phase synchrony in cortical networks with neuronal avalanches. *J. Neurosci.* **32**, 1061–1072 (2012).
33. J. Liang, T. Zhou, C. Zhou, Hopf bifurcation in mean field explains critical avalanches in excitation-inhibition balanced neuronal networks: A mechanism for multiscale variability. *Front. Syst. Neurosci.* **14**, 87 (2020).
34. P. Villegas, P. Moretti, M. A. Muñoz, Frustrated hierarchical synchronization and emergent complexity in the human connectome network. *Sci. Rep.* **4**, 1–7 (2014).
35. V. Buendía, P. Villegas, R. Burioni, M. A. Muñoz, Hybrid-type synchronization transitions: Where incipient oscillations, scale-free avalanches, and bistability live together. *Phys. Rev. Res.* **3**, 023224 (2021).
36. A. Steyn-Ross, M. Steyn-Ross, *Modeling Phase Transitions in the Brain* (Springer, 2010), vol. 509.
37. D. Dahmen, S. Grün, M. Diesmann, M. Helias, Second type of criticality in the brain uncovers rich multiple-neuron dynamics. *Proc. Natl. Acad. Sci. U.S.A.* **116**, 13051–13060 (2019).
38. G. Tkačik *et al*., Thermodynamics and signatures of criticality in a network of neurons. *Proc. Natl. Acad. Sci. U.S.A.* **112**, 11508–11513 (2015).
39. T. Petermann *et al*., Spontaneous cortical activity in awake monkeys composed of neuronal avalanches. *Proc. Natl. Acad. Sci. U.S.A.* **106**, 15921–15926 (2009).
40. Z. Ma, G. G. Turrigiano, R. Wessel, K. B. Hengen, Cortical circuit dynamics are homeostatically tuned to criticality in vivo. *Neuron* **104**, 655–664 (2019).
41. A. J. Fontenele *et al*., Criticality between cortical states. *Phys. Rev. Lett.* **122**, 208101 (2019).
42. S. S. Poil, R. Hardstone, H. D. Mansvelder, K. Linkenkaer-Hansen, Critical-state dynamics of avalanches and oscillations jointly emerge from balanced excitation/inhibition in neuronal networks. *J. Neurosci.* **32**, 9817–9823 (2012).
43. J. M. Palva *et al*., Neuronal long-range temporal correlations and avalanche dynamics are correlated with behavioral scaling laws. *Proc. Natl. Acad. Sci. U.S.A.* **110**, 3585–3590 (2013).
44. J. Cabral, M. L. Kringelbach, G. Deco, Functional connectivity dynamically evolves on multiple time scales over a static structural connectome: Models and mechanisms. *NeuroImage* **160**, 84–96 (2017).
45. E. Tagliazucchi, P. Balenzuela, D. Fraiman, D. R. Chialvo, Criticality in large-scale brain fMRI dynamics unveiled by a novel point process analysis. *Front. Physiol.* **3**, 15 (2012).
46. R. Wang *et al*., Hierarchical connectome modes and critical state jointly maximize human brain functional diversity. *Phys. Rev. Lett.* **123**, 038301 (2019).
47. J. Liang, C. Zhou, Criticality enhances the multilevel reliability of stimulus responses in cortical neural networks. *PLoS Comput. Biol.* **18**, e1009848 (2022).
48. E. D. Fagerholm *et al*., Neural systems under change of scale. *Front. Comput. Neurosci.* **15**, 33 (2021).
49. L. Meshulam, J. L. Gauthier, C. D. Brody, D. W. Tank, W. Bialek, Coarse graining, fixed points, and scaling in a large population of neurons. *Phys. Rev. Lett.* **123**, 178103 (2019).
50. L. Meshulam, J. L. Gauthier, C. D. Brody, D. W. Tank, W. Bialek, Coarse–graining and hints of scaling in a population of 1000+ neurons. arXiv [Preprint] (2018). http://arxiv.org/abs/1812.11904. (Accessed 26 April 2022).
51. S. Bradde, W. Bialek, PCA meets RG. *J. Stat. Phys.* **167**, 462–475 (2017).
52. N. A. Steinmetz, P. Zatka-Haas, M. Carandini, K. D. Harris, Distributed coding of choice, action and engagement across the mouse brain. *Nature* **576**, 266–273 (2019).
53. M. C. Morrell, A. J. Sederberg, I. Nemenman, Latent dynamical variables produce signatures of spatiotemporal criticality in large biological systems. *Phys. Rev. Lett.* **126**, 118302 (2021).
54. G. Nicoletti, S. Suweis, A. Maritan, Scaling and criticality in a phenomenological renormalization group. *Phys. Rev. Res*. **2**, 023144 (2020).
55. Y. Hu, H. Sompolinsky, The spectrum of covariance matrices of randomly connected recurrent neuronal networks. bioRxiv (2020).
56. J. Bun, J. P. Bouchaud, M. Potters, Cleaning large correlation matrices: Tools from random matrix theory. *Phys. Rep.* **666**, 1–109 (2017).
57. I. A. Davidovich, Y. Roudi, Bayesian interpolation for power laws in neural data analysis. arXiv [Preprint] (2022). http://arxiv.org/abs/2204.08525 (Accessed 26 April 2022).
58. J. Shlens, A tutorial on principal component analysis. arXiv [Preprint] (2014). http://arxiv.org/abs/1404.1100 (Accessed 26 April 2022).
59. P. Gao, S. Ganguli, On simplicity and complexity in the brave new world of large-scale neuroscience. *Curr. Opin. Neurobiol.* **32**, 148–155 (2015).
60. A. Renart *et al*., The asynchronous state in cortical circuits. *Science* **327**, 587–590 (2010).
61. V. Pernice, B. Staude, S. Cardanobile, S. Rotter, How structure determines correlations in neuronal networks. *PLOS Comput. Biol*. **7**, e1002059 (2011).
62. J. Trousdale, Y. Hu, E. Shea-Brown, K. Josić, Impact of network structure and cellular response on spike time correlations. *PLOS Comput. Biol.* **8**, e1002408 (2012).
63. G. K. Ocker *et al*., From the statistics of connectivity to the statistics of spike times in neuronal networks. *Curr. Opin. Neurobiol.* **46**, 109–119 (2017).
64. L. Tiberi *et al*., Gell-Mann-Low criticality in neural networks. *Phys. Rev. Lett.* **128**, 168301 (2022).
65. M. E. Rule, T. O'Leary, C. D. Harvey, Causes and consequences of representational drift. *Curr. Opin. Neurobiol.* **58**, 141–147 (2019).
66. J. A. Harris *et al*., Hierarchical organization of cortical and thalamic connectivity. *Nature* **575**, 195–202 (2019).
67. L. Aitchison, N. Corradi, P. E. Latham, Zipf's law arises naturally when there are underlying, unobserved variables. *PLoS Comput. Biol.* **12**, e1005110 (2016).
68. D. J. Schwab, I. Nemenman, P. Mehta, Zipf's law and criticality in multivariate data without fine-tuning. *Phys. Rev. Lett.* **113**, 068102 (2014).
69. J. D. Semedo, A. Zandvakili, C. K. Machens, M. Y. Byron, A. Kohn, Cortical areas interact through a communication subspace. *Neuron* **102**, 249–259 (2019).
70. G. B. Morales, M. A. Muñoz, Optimal input representation in neural systems at the edge of chaos. *Biology* **10**, 702 (2021).
71. G. Tanaka *et al*., Recent advances in physical reservoir computing: A review. *Neural Netw.* **115**, 100–123 (2019).
72. C. G. Langton, Computation at the edge of chaos: Phase transitions and emergent computation. *Phys. D: Nonlinear Phenomena* **42**, 12–37 (1990).
73. N. Bertschinger, T. Natschläger, Real-time computation at the edge of chaos in recurrent neural networks. *Neural Comput.* **16**, 1413–1436 (2004).
74. J. Boedecker, O. Obst, J. T. Lizier, N. M. Mayer, M. Asada, Information processing in echo state networks at the edge of chaos. *Theory Biosci.* **131**, 205–213 (2012).
75. A. Clauset, C. R. Shalizi, M. E. Newman, Power-law distributions in empirical data. *SIAM Rev.* **51**, 661–703 (2009).